

RECONSTRUCTION OF THE HUMAN HIPPOCAMPUS IN 3D FROM HISTOLOGY AND HIGH-RESOLUTION EX-VIVO MRI

Daniel H. Adler, Alex Yang Liu, John Pluta, Salmon Kadivar, Sylvia Orozco, Hongzhi Wang, James C. Gee, Brian B. Avants, Paul A. Yushkevich

Penn Image Computing and Science Laboratory,
Department of Radiology, University of Pennsylvania, Philadelphia, PA, USA

ABSTRACT

In this paper, we present methods for the reconstruction of 3D histological volumes of the human hippocampal formation from histology slices. Inter-slice alignment is guided by a graph-theoretic approach that minimizes the impact of badly distorted slices. The reconstruction is refined by iterative affine and deformable co-registration with a high-resolution MRI of the postmortem tissue sample. We present an evaluation of reconstruction accuracy that is based on measures of similarity between boundaries drawn on both histology and MRI. Our methodology is currently being applied to an MRI atlas of the human hippocampal formation, in which atlas anatomical labels are derived from segmentation of reconstructed histology.

Index Terms— Hippocampus, histology, reconstruction, segmentation, registration

1. INTRODUCTION

The human hippocampal formation (HF) consists of several structures of the medial temporal lobe that play important roles in declarative memory. The formation is defined to comprise the hippocampus proper, as well as the main structures to which its neurons are connected. The HF is divided into microscopically-defined anatomical subregions that serve different roles in the memory system and that are differentially affected by processes of aging and neurodegenerative diseases [1], such as in Alzheimer's Disease (AD) [2].

The motivating application for this paper is the generation of a computational atlas of the HF that describes its anatomical variability. We have performed ultra-high resolution MR imaging at 9.4 T on 25 intact, postmortem HF samples. These images will be spatially normalized using deformable modeling techniques to construct the reference image of the atlas, as has been done using five sample in a proof-of-concept atlas [3].

Following MRI, a subset of the postmortem HF tissue samples is sectioned, histologically stained, and scanned at micron resolution. The purpose of this paper is to describe the reconstruction of 3D volumes from these sections, which will serve as the primary source for labeling structures in our atlas, including the hippocampal subfields. While MRI is advantageous for studying neuroanatomy in 3D, it cannot match the level of microscopic detail visible on histology, which can be used to delineate regions based on cellular features. Other groups have also leveraged histology for atlas boundary delineation, such as for the human basal ganglia [4].

At its most basic level, reconstruction can be reduced to 2D inter-slice registration followed by slice stacking. In practice, however, this often leads to discontinuous results due to poor registration between distorted sections (e.g. tissue stretching, tearing, and displacement during microtomy). Even small misalignments between neighbouring slices can accumulate, distorting shapes along the stacking dimension. The shape information lost during sectioning can be minimized with smoothness constraints or reintroduced via co-registration to another modality, such as MRI or block-face imaging. Many registration techniques have been used for reconstruction, ranging from manual alignment with landmarks to automated rigid, affine, block-matching, free-form deformation, and diffeomorphic transformation models. More detailed reviews of histology reconstruction methods are given in [5, 6, 7].

The methods that we use are based on our group's prior work to reconstruct whole mouse brain histology for the anatomical reference image of the Allen Brain Atlas [8]: a genome-wide map of gene expression in the mouse brain that is freely accessible online [9]. There are two main distinguishing aspects of these methods. First, a least-cost sequence of transformations is found between each slice and a reference slice using a graph-theoretic approach, thereby minimizing the impact of imaging artifacts and distortions. Second, iterative affine and diffeomorphic co-registration with MRI are used to refine the reconstruction. This improves the 3D continuity and accuracy of anatomical structures in the histology volume. The final result is a smooth reconstruction that is co-registered to its accompanying MRI.

This project is supported by NIH grants R01 AG037376, K25 AG027785 and K25-AG027785-03S1, an NSERC Canada Graduate Scholarship, and the HHMI Interfaces program

2. MATERIALS AND METHODS

2.1. Specimens and imaging

We studied a formalin-fixed brain specimen from an autopsy case with no abnormal neuropathological findings that was obtained from the National Disease Research Interchange (NDRI) National Resource Center (Philadelphia, PA). We extracted a tissue sample containing the intact hippocampal formation from the right hemisphere, measuring approximately $2 \times 3 \times 8 \text{ cm}^3$. Imaging was performed on a 9.4 T Varian, 31 cm horizontal bore scanner using a 70 mm ID TEM transmit/receive volume coil, with the tissue sample immersed in a cylinder of Fomblin. A standard spin echo multi-slice (SEMS) sequence was acquired along an oblique slice plane parallel to the long axis of the hippocampus, with TR/TE = 5 s/23 ms, 48 signal averages. The image had $200 \times 500 \times 128$ voxels with 0.16 mm^3 isotropic resolution.

Next, the tissue sample was cut into six blocks oriented perpendicular to the long axis of the HF. An MRI was acquired of each block using the SEMS sequence with TR/TE = 4 s/23 ms, 80 signal averages, and 0.20 mm^3 isotropic resolution. Following MRI, the blocks underwent histological processing. The tissue was embedded in paraffin and sectioned on a microtome into $5 \mu\text{m}$ thick slices parallel to the block face. Histology slice spacing was $200 \mu\text{m}$, so as to match the MRI spacing. Sections were placed on slides and histochemically stained using the Kluver-Barrera method (luxol fast blue counterstained with cresyl violet), which highlights the Nissl substance in neuronal cell bodies as pink-violet, and myelin in axons as blue-green. The slides were scanned at $0.5 \mu\text{m}/\text{pixel}$ with an Aperio ScanScope CS system.

2.2. Histology pre-processing

To make the processing workload more manageable, the digitized slides were converted to grayscale and downsampled to 1% of their original size in each dimension ($50 \mu\text{m}/\text{pixel}$). All subsequent processing steps were performed on the downsampled grayscale images, as they retained high contrast of salient anatomical structures and a sufficient level of detail to guide reconstruction. To prevent image background artifacts (e.g. dislodged tissue fragments, stains, and other debris) from influencing subsequent image registration, the HF tissue was segmented from background in each slice using an active contour level set algorithm, retaining only the largest connected component of each sample. Histogram equalization was also performed between the histology images from each tissue block.

2.3. Graph-theoretic slice stacking

The first stage of our pipeline is histology inter-slice co-registration and stacking to a 3D volume. We minimize the propagation of alignment errors and the accumulation

of small slice shifts along the stacking (or z) dimension using the following approach [8]. Let us denote the ordered sequence of histology slices as $\{h_1, \dots, h_N\}$. First, each histology slice h_i is co-registered to its k neighbouring slices $\{h_{i+1}, \dots, h_{i+k}\}$ using 2D affine transformations (we set $k = 5$). Next, we construct a weighted graph with N vertices and edge weights set to $w_{ij} = w_{ji} = (1 + \text{NMI}(h_i, h_j))|i - j|(1 + \epsilon)^{|i-j|}$, where $\text{NMI}(h_i, h_j)$ is the optimal normalized mutual information (NMI) similarity metric between the two slices after registration, normalized to the range $[0, 1]$ (smaller values corresponding to better registration). The positive constant ϵ modulates the amount of slice skipping: smaller values reduce skipping, and hence tend to increase registration error propagation; larger values of ϵ increase slice skipping, disturbing alignment between neighbouring slices in the reconstruction. We set $\epsilon = 1$, assigning greater weight to more distant slice pairs.

One slice is then designated as the reference, and the lowest cost path is found to it from every other slice using Dijkstra's algorithm. The path between two slices represents the optimal sequence of 2D affine transformations between them, taking both the similarity metric and slice proximity into account. Finally, the optimal sequence of transformations for each slice is concatenated into a single transformation. All slices are then warped to the reference slice and stacked into a volume. This algorithm effectively bypasses slices that are dissimilar to their neighbours, thus avoiding their negative effects on reconstruction.

2.4. Histology-MRI co-registration refinement

Inter-slice alignment gives good correspondence between local histology features and yields an initial estimate of reconstructed tissue. However, the histology fails to exactly match the 3D tissue shape (see Fig. 2). To eliminate this so-called z -shift error, we co-register histology and MRI, the latter of which is assumed to represent ground truth 3D tissue shape.

Let us call H the histology volume following stacking in the previous step (sec. 2.3) and M the MRI volume. First, M is registered to H using the NMI similarity metric and a 3D affine transformation model, which accounts for global positioning and shape differences between the two modalities (e.g. due to shrinking of the tissue during fixation). Let us denote by M^* the MRI volume after it has been transformed and resampled to the space of H . Two-dimensional affine registrations using NMI are then performed between each slice of H and its corresponding slice of M^* . The transformed slices of H are then re-stacked into a new estimate of the histology volume, which we call H^* . We iterate this 3D/2D registration sequence (i.e. mapping M to H^* , etc.) until the relative change in NMI metric between histology and MRI slices falls below 10^{-6} : about four iterations until convergence.

2.5. Diffeomorphic registration refinement

As a final step, we perform deformable registration between the histology and MRI slices. The co-registered volumes H^* and M^* from the last step (sec. 2.4) are used as input. Each histology slice h_i is deformed towards its neighbours h_{i-1} and h_{i+1} , as well as to its corresponding MRI slice m_i . In particular, the similarity metric for this registration is $a \cdot \text{NMI}(h_{i-1}, h_i) + a \cdot \text{NMI}(h_i, h_{i+1}) + \text{NMI}(h_i, m_i)$. We use a weight of $a = 0.1$, which favours matching to the MRI while preserving continuity between histology slices. The registrations are done using a symmetric 2D diffeomorphic transformation model (SyN) in the Advanced Normalization Tools (ANTs) toolkit [10], which we use to perform all registrations in our pipeline. We iterate over all slices until the relative change in NMI metric between the histology and MRI volumes falls below 0.5×10^{-5} (approximately 15-25 iterations). Deformable registration greatly improves the continuity of anatomical structures between slices of the reconstruction.

2.6. Evaluation of reconstruction accuracy

To evaluate reconstruction accuracy, we measured the similarity of two corresponding anatomical boundaries in the histology and MRI volumes. The boundaries that are chosen reliably appear with high contrast in both modalities [11]. The first boundary separates the hippocampal gray matter of the stratum pyramidale from the white matter of the alveus and stratum oriens. This boundary runs parallel to the hippocampal fissure and essentially defines the outermost extent of the gray matter in the hippocampus proper. The second boundary is the interface of dentate gyrus (DG) gray matter with the so-called ‘dark band’. The dark band is formed by the molecular, lacunosum and radiatum cell layers.

The boundaries were drawn by a human rater on all colour histology slides and on the original MRI blocks. Boundary

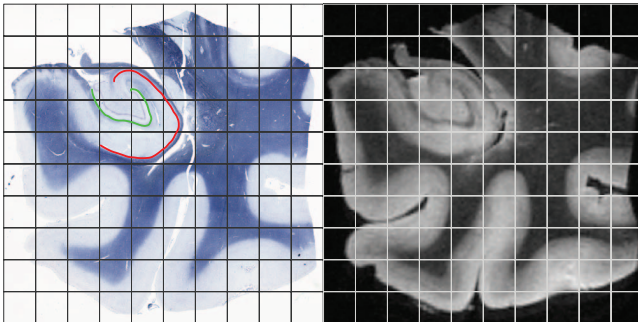


Fig. 1. Corresponding coronal histology (left) and MRI (right) sections following diffeomorphic reconstruction refinement. Evaluation boundaries are shown for the hippocampus (red) and dark band (green).

displacement error was calculated between reconstructed histology and MRI:

$$\text{BDE}(A, B) = \left(\frac{1}{|A|} \sum_{p \in A} d(p, B)^2 + \frac{1}{|B|} \sum_{p \in B} d(p, A)^2 \right)^{\frac{1}{2}},$$

where A and B denote the sets of points in two boundaries and $d(p, A)$ is the Euclidean distance from point p to the closest point on boundary A .

2.7. Histology segmentation

Three raters manually delineated seven HF anatomical structures on all full-resolution histology slides using cytoarchitectural features: entorhinal cortex (EC), pre/parasubiculum, subiculum (SUB), dentate gyrus (DG), and Cornu Ammonis (CA) 1/2/3 subfields. Segmentations focussed on accurately defining transitions between structures. A consensus segmentation between raters was obtained using the simultaneous truth and performance level estimation (STAPLE) algorithm.

3. RESULTS

Figure 1 depicts the final results of reconstruction following diffeomorphic registration refinement. Matching slices containing the hippocampus body (and other medial temporal lobe structures) are shown in MRI and histology. Anatomical features are seen to visually match quite well. Boundaries of the hippocampus and dark band, used for validation, are overlaid on the histology.

A comparison of histology reconstruction following graph-theoretic slice stacking (sec. 2.3) and diffeomorphic refinement (sec. 2.5) are shown in Fig. 2. Slices are generally aligned in the initial reconstruction, but features are not continuous in the stacking (z) direction. Co-registration with MRI and diffeomorphic refinement with shape averaging significantly improve visual reconstruction quality. This observation is quantified in Fig. 3, which shows that the error between corresponding anatomical boundaries in histology and MRI decreases following reconstruction refinement steps.

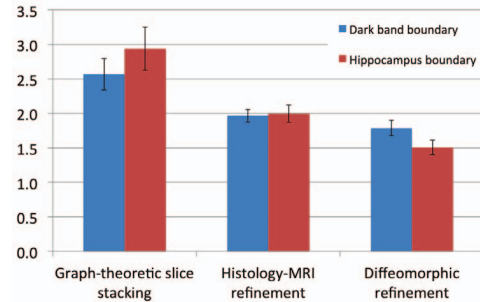


Fig. 3. Mean displacement errors between boundaries in histology volumes and MRI following the reconstruction stages

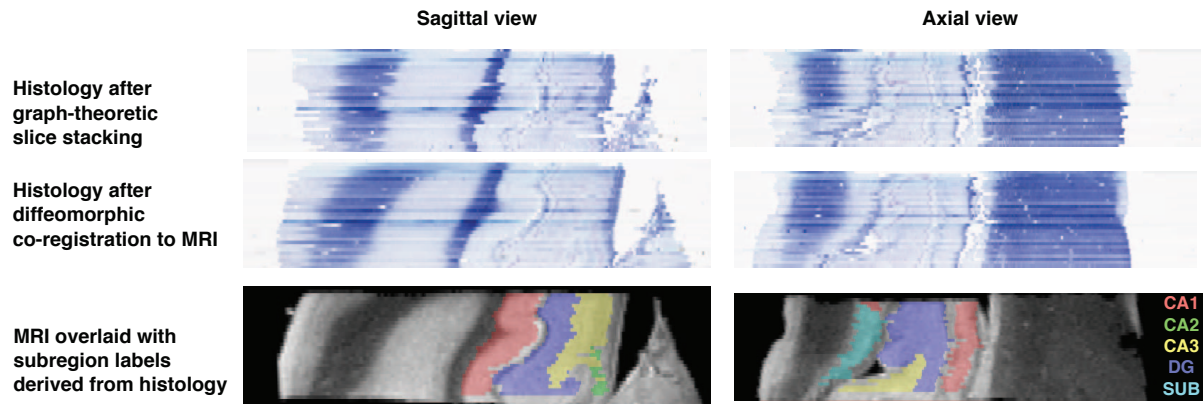


Fig. 2. Side-view comparisons of reconstructed histology volumes after slice stacking and diffeomorphic refinement. Manual segmentations from histology are warped and overlaid on corresponding MRI sections: dentate gyrus (DG), subiculum (SUB).

4. DISCUSSION

Reconstruction of mouse whole brain histology for the Allen Brain Atlas [8] and human hippocampus in the present work are similar in many ways. However, the mouse brain MRI had low resolution and contrast, limiting the extent to which its features could guide reconstruction. The present MRI is of very high resolution (0.20 mm^3) and contrast, making it possible to directly match some internal features with histology. Yet even at very high resolution, MRI does not show enough detail to accurately define boundaries between some structures. Consequently, in our previous hippocampus atlas, boundaries between subfields and other regions were based on rules defined by shape and position relative to landmarks [3].

We will augment the next version of our atlas with reconstructed histology, serving as the primary source for reliably labeling structures. The atlas could serve as a valuable resource for *in vivo* neuroimaging studies of structure and function by providing prior knowledge on the distributions of HF structures. For instance, it could serve as an anatomical model for *in vivo* MRI segmentation, thereby allowing us to describe volume and shape changes at the subfield level. In AD clinical pharmaceutical trials, this may lead to more sensitive and specific biomarkers of hippocampal atrophy than are possible with whole-hippocampus measures, leading to better cohort selection and treatment effect monitoring.

5. REFERENCES

- [1] S.A. Small et al., “A pathophysiological framework of hippocampal dysfunction in ageing and disease,” *Nature Rev Neurosci*, vol. 12, no. 10, pp. 585–601, 2011.
- [2] S.G. Mueller and M.W. Weiner, “Selective effect of age, Apo E4, and Alzheimer’s disease on hippocampal subfields,” *Hippocampus*, vol. 19, no. 6, pp. 558–564, 2009.
- [3] P.A. Yushkevich et al., “A high-resolution computational atlas of the human hippocampus from postmortem magnetic resonance imaging at 9.4T,” *NeuroImage*, vol. 44, no. 2, pp. 385–398, 2009.
- [4] J. Yelnik et al., “A three-dimensional, histological and deformable atlas of the human basal ganglia. I. Atlas construction based on immunohistochemical and MRI data,” *NeuroImage*, vol. 34, no. 2, pp. 618–638, 2007.
- [5] O. Schmitt et al., “Image registration of sectioned brains,” *Int J Comput Vision*, vol. 73, no. 1, pp. 5–39, 2007.
- [6] I. Arganda-Carreras et al., “Non-rigid consistent registration of 2D image sequences,” *Phys Med Biol*, vol. 55, no. 20, pp. 6215–6242, 2010.
- [7] C. Ceritoglu et al., “Large deformation diffeomorphic metric mapping registration of reconstructed 3D histological section images and *in vivo* MR images,” *Front Hum Neurosci*, vol. 4, no. 43, 2010.
- [8] P.A. Yushkevich et al., “3D mouse brain reconstruction from histology using a coarse-to-fine approach,” in *WBIR*, 2006, vol. 4057 of *LNCS*, pp. 230–237.
- [9] E.S. Lein et al., “Genome-wide atlas of gene expression in the adult mouse brain,” *Nature*, vol. 445, pp. 168–176, 2007.
- [10] B.B. Avants et al., “Symmetric diffeomorphic image registration with cross-correlation: Evaluating automated labeling of elderly and neurodegenerative brain,” *Med Image Anal*, vol. 12, no. 1, pp. 26–41, 2008.
- [11] G.M. Fatterpekar et al., “Cytoarchitecture of the human cerebral cortex: MR microscopy of excised specimens at 9.4 Tesla,” *Am J Neuroradiol*, vol. 23, no. 8, pp. 1313–1321, 2002.